Inorganic Chemistry

Article

pubs.acs.org/IC

Terbium(III) and Yttrium(III) Complexes with Pyridine-Substituted Nitronyl Nitroxide Radical and Different β-Diketonate Ligands. Crystal Structures and Magnetic and Luminescence Properties

Anthony Lannes,[†] Mourad Intissar,[‡] Yan Suffren,[‡] Christian Reber,*[,‡] and Dominique Luneau*[,†]

[†]Laboratoire des Multimatériaux et Interfaces (UMR 5616), Université Claude Bernard Lyon 1, Campus de la Doua, 69622, Villeurbanne Cedex, France

[‡]Département de chimie, Université de Montréal, Montréal, Québec H3C 3J7, Canada

Supporting Information

ABSTRACT: A terbium(III) complex of nitronyl nitroxide free radical 2-(2-pyridyl)-4,4,5,5-tetramethyl-4,5-dihydro1*H*-imidazolyl-1-oxy-3-oxide (NIT2Py), [Tb(acac)3NIT2Py]·0.5H_2O (**3**) (acac = acetylacetonate), was synthesized for comparison with the previously reported [Tb(hfac)$_3$NIT2Py]·0.5C_7H_{16} (**1**) (hfac = hexafluoroacetylacetonate), together with their yttrium analogues [Y(hfac)$_3$NIT2Py]·0.5C_7H_{16} (**2**) and [Y(acac)$_3$NIT2Py]·0.5H_2O (**4**). The crystal structures show that in all complexes the nitronyl nitroxide radical acts as a chelating ligand. Magnetic studies show that **3** like **1** exhibits slow relaxation of magnetization at low temperature, suggesting single-molecule magnet behavior. The luminescence spectra show resolved vibronic structure with the main interval decreasing from 1600 cm^{-1} to 1400 cm^{-1} between 80 and 300 K. This effect is analyzed quantitatively using experimental Raman frequencies.

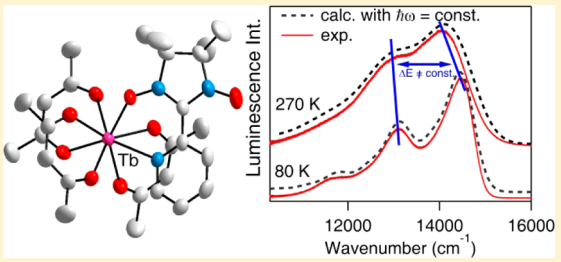

INTRODUCTION

Single-molecule magnets (SMMs) have attracted more and more attention since their discovery.[1] At first, the design of coordination compounds that exhibit slow relaxation of the magnetization has mainly dealt with increasing the ground state spin of polynuclear compounds based on 3d elements.[2,3] The discovery that single-ion complexes of lanthanide with unquenched orbital angular momentum may show SMM behavior has established magnetic anisotropy as a main factor.[4,5] Following this has opened the way to the synthesis of numerous compounds made of only lanthanide ions or combined with 3d metal ions to instill anisotropy in high-spin clusters.[6−10] This has resulted in the discovery of many compounds exhibiting large energy barriers for the reversal of the magnetization.[11−13] Some actinide complexes have also been found to show SMM behavior.[14−20] However, the blocking temperatures are still observed at very low temperature, and one's main focus nowadays is to understand the magneto-structural correlations to guide the synthesis work. This mainly involves theoretical calculations[8] with complementary experimental techniques such as EPR,[21−24] polarized neutron diffraction,[25] or NMR.[26,27] Studies of the optical properties is also helpful to molecular magnetism, as we have shown previously,[28−34] and have become pervasive in recent studies of lanthanide-based SMMs.[35−39,40] Complementary to these approaches is to compare series of related compounds that show subtle differences in magnetic behavior.[41]

Nitronyl nitroxide (NIT) radicals are a unique type of stable and versatile free radicals that have been popular magnetic building blocks of molecular-based magnetic materials.[42−46] Comparatively they have been almost forgotten in the course to SMMs.[41,47−53] However, recent discoveries of a peculiar enhancement of the energy barrier for reversal of magnetization in dinuclear lanthanide complexes with bridging dinitrogen[54,55] and bipyrimidyl[56] radicals have shown that the metal−radical may also be promising for SMMs.

Herein we report the comparative study of two Tb-radical complexes based on the same nitronyl nitroxide radical (NIT2Py) as shown in Figure 1 but with hexafluoroacetylacetonate (hfac) or acetylacetonate (acac) as ancillary ligand, respectively: [Tb(hfac)$_3$NIT2Py]0.5C_7H_{16} (**1**), which was previously reported by L.-C. Li,[57] and [Tb(acac)$_3$NIT2Py]·0.5H_2O (**3**), which is new, together with their yttrium analogues [Y(hfac)$_3$NIT2Py]·0.5C_7H_{16} (**2**) and [Y(acac)$_3$NIT2Py]·0.5H_2O (**4**). Magnetic studies show that **3**

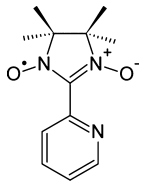

Figure 1. Chemical structure of the nitronyl nitroxide radical NIT2Py.

Received: April 7, 2014

   dx.doi.org/10.1021/ic500779y | *Inorg. Chem.* XXXX, XXX, XXX−XXX

Table 1. Crystal Data for $Tb(hfac)_3NIT2Py{\cdot}0.5C_7H_{16}$ (1), $Y(hfac)_3NIT2Py{\cdot}0.5C_7H_{16}$ (2), $Tb(acac)_3NIT2Py{\cdot}0.5H_2O$ (3), and $Y(acac)_3NIT2Py{\cdot}0.5H_2O$ (4)

	1[a]	2	3	4
formula	$TbC_{30.5}H_{27}O_8N_3F_{18}$	$Y_2C_{61}H_{54}O_{16}N_6F_{36}$	$Tb_2C_{54}H_{76}N_6O_{17}$	$Y_2C_{54}H_{76}N_6O_{17}$
M (g/mol)	1064.47	1988.92	1399.08	1259.03
cryst shape, color	chunk, pink red	chunk, dark red	needle, dark violet	polyhedron, violet
cryst size (mm)	0.10 × 0.03 × 0.02	0.08 × 0.08 × 0.08	0.132 × 0.256 × 0.983	0.126 × 0.270 × 0.406
cryst syst	monoclinic	triclinic	monoclinic	monoclinic
space group (no.)	$P2_1/n$ (#14)	$P\bar{1}$ (#2)	$C2/c$ (#15)	$C2/c$ (#15)
T (K)	150	100	293	293
λ(Kα Cu) (Å)	1.541 78	1.541 78		
λ(Kα Mo) (Å)			0.710 73	0.710 73
a (Å)	16.298(1)	14.4468(13)	27.5929(7)	27.5452(13)
b (Å)	12.8383(3)	15.0836(13)	14.5138(3)	14.5077(5)
c (Å)	20.5399(13)	18.8539(3)	19.3570(6)	19.3707(10)
α (Å)	90	102.465(4)	90	90
β (Å)	110.724(3)	102.943(4)	114.947(3)	114.902(6)
γ (Å)	90	92.014(5)	90	90
V (Å^3)	4019.7(4)	3894.6(6)	7028.8(4)	7021.2(6)
Z	4	2	4	4
D (g/cm^3)	1.759	1.696	1.322	1.191
μ (mm^{-1})	9.889	3.387	2.057	1.706
F(000)	2088	1984	2832	2624
θ range (deg)	3.0−69.8	2.5−71.7	2.9−29.4	2.9−29.4
reflns (h k l)	$-19 \le 19$	$-17 \le 17$	$-37 \le 32$	$-37 \le 32$
	$-15 \le 15$	$-18 \le 18$	$0 \le 18$	$0 \le 19$
	$-24 \le 24$	$-23 \le 23$	$0 \le 26$	$0 \le 24$
no. of reflns	79 557	102 315	8397	8395
no. of indep reflns	7510	14 567	5961	4643
no. of params	693	1135	359	357
R_{int}	0.100	0.065	0.029	0.062
R1[b]	0.0523	0.0788	0.0358	0.0571
wR2[c]	0.1437	0.2194	0.0410	0.0674
GOF on F^2	1.035	1.025	1.0608	1.059
$\Delta\rho_{max}/\Delta\rho_{min}$ (e·Å^{-3})	0.463/−1.450	2.182/−1.082	1.08/−0.85	0.51/−0.42

[a]For comparison with ref 51. [b]$R1 = \sum||F_o| - |F_c||/\sum|F_o|$. [c]$wR2 = [\sum(w(F_o^2 - F_c^2)^2)/\sum(w(F_o^2)^2)]^{1/2}$ with $w = 1/[(\sigma^2F_o^2) + (aP)^2 + bP]$ and $P = (\max(F_o^2) + 2F_c^2)/3$.

like **1** exhibits slow relaxation of magnetization at low temperature, suggesting single-molecule magnet behavior. Luminescence spectra for all four complexes have been measured on crystalline samples. They show band shapes similar to the uncoordinated NIT2Py previously reported by us[29] but with small shifts and vibronic structure with unusual temperature-dependent variations. This was analyzed using the time-dependent theory of electronic spectroscopy and experimental Raman frequencies.[58]

EXPERIMENTAL SECTION

Materials. All reactions were conducted in aerobic conditions. All reagents were obtained from commercial sources and used as received. 2,3-Bis(hydroxylamino)-2,3-dimethylbutane[59] and nitronyl nitroxide free radical 2-(2-pyridyl)-4,4,5,5-tetramethyl-4,5-dihydro1*H*-imidazol-yl-1-oxy-3-oxide (NIT2Py) have been synthesized as previously reported.[60]

Synthesis of Complexes. *$[M(hfac)_3(H_2O)_2]$[61] with M = Tb^{III} or Y^{III}.* A 5 g amount of hexafluoroacetylacetone stored in a refrigerator was added to 15 mL of cold water. The mixture was stirred strongly for 30 min, then kept in the refrigerator for 3 days to give $[hfac{\cdot}2H_2O]$ as a solid, which was isolated by filtration. Then 200 mg (0.81 mmol) of this solid was dissolved in 100 mL of diethyl ether, and 126 μL of ammonia (25%) was added under stirring. The resulting solution was then mixed with a solution of $TbCl_3{\cdot}6H_2O$ (100 mg, 0.29 mmol) or $YCl_3{\cdot}6H_2O$ (82 mg, 0.29 mmol) in 10 mL of H_2O. The aqueous phase was then extracted with 2 × 50 mL of diethyl ether. The organic phase was dried with sodium sulfate, then filtered and evaporated at room temperature to give the title compound in 75% yield.

$[M(hfac)_3NIT2Py{\cdot}0.5C_7H_{16}]$[51,62] with M = Tb^{III} (1) or Y^{III} (2). A suspension of 100 mg of $[M(hfac)_3(H_2O)_2]$ was prepared in 10 mL of heptane and boiled at 90 °C for 1 h until total dissolution of the complex. The heating was stopped, and a few drops of dichloromethane were added to avoid crystallization upon cooling. When this solution was cool enough (<30 °C), 27 mg (0.12 mmol) or 32 mg (0.13 mmol) of NIT2Py respectively for the Tb and Y compounds previously dissolved in a minimum of dichloromethane was added. After 1 week, slow evaporation of the solvent gave single crystals as dark violet blocks. Yield: 60%.

$[M(acac)_3NIT2Py{\cdot}0.5H_2O]$ with M = Tb^{III} (3) or Y^{III} (4). A 100 mg portion of of $M(acac)_3{\cdot}3H_2O$ (M = Tb, 509.92 g/mol, 0.196 mmol; M = Y, 439.9 g/mol, 0.227 mmol) was dissolved in a 10 mL mixture of dichloromethane/heptane (3:7). After dissolution by stirring, 40 mg (0.17 mmol) or 46 mg (0.19 mmol) of NIT2Py respectively for the Tb and Y compounds, previously dissolved in a minimum of dichloromethane, was added. The resultant solution was then stirred for 1 h, and three drops of water were slowly added. The solution was left undisturbed for slow evaporation of the solvent at room temperature. After 2 days, small single crystals were collected as dark violet sticks. Yield: 25%.

Crystal Structure Determination. Single crystals of $[Tb(hfac)_3NIT2Py]{\cdot}0.5C_7H_{16}$ (**1**) and $[Y(hfac)_3NIT2Py]{\cdot}0.5C_7H_{16}$ (**2**) were mounted on a Bruker SMART 6000 diffractometer with optics,

dx.doi.org/10.1021/ic500779y | Inorg. Chem. XXXX, XXX, XXX−XXX

Table 2. Metal−Ligand Bond Lengths (Å) in 1 and 2

atoms	distance	atoms	distance	atoms	distance	atoms	distance	atoms	distance
Tb1−O1	2.313(4)	Y1−O11	2.258(5)	Y2−O21	2.270(5)	Tb1−O11	2.323(3)	Y1−O8	2.299(3)
Tb1−O8	2.323(4)	Y1−O17	2.296(5)	Y2−O26	2.297(5)	Tb1−O8	2.324(3)	Y1−O11	2.302(3)
Tb1−O5	2.330(4)	Y1−O16	2.321(5)	Y2−O24	2.309(5)	Tb1−O10	2.327(3)	Y1−O10	2.306(3)
Tb1−O4	2.360(3)	Y1−O13	2.325(5)	Y2−O28	2.310(5)	Tb1−O9	2.331(3)	Y1−O9	2.309(2)
Tb1−O6	2.375(4)	Y1−O14	2.328(5)	Y2−O27	2.317(5)	Tb1−O7	2.352(3)	Y1−O7	2.329(3)
Tb1−O7	2.375(4)	Y1−O15	2.328(5)	Y2−O23	2.332(6)	Tb1−O12	2.364(3)	Y1−O12	2.342(3)
Tb1−O3	2.378(4)	Y1−O18	2.365(5)	Y2−O25	2.381(6)	Tb1−O5	2.405(3)	Y1−O5	2.380(3)
Tb1−N3	2.587(4)	Y1−N13	2.609(6)	Y2−N23	2.625(6)	Tb1−N4	2.700(3)	Y1−N4	2.689(3)

equipped with a monochromatic copper Cu Kα radiation source (λ = 1.547 18 Å) at 100 and 150 K, respectively. Cell refinement and data reduction were performed using APEX2.[63] Absorption corrections were applied using SADABS.[64] Structures were solved by direct methods using SHELXS97 and refined on F^2 by full-matrix least-squares using SHELXL97.[65] All non-hydrogen atoms were refined anisotropically. Hydrogen atoms were refined on calculated positions using a riding model.

Single-crystal X-ray studies of [Tb(acac)$_3$NIT2Py]·0.5H$_2$O (**3**) and [Y(acac)$_3$NIT2Py]·0.5H$_2$O (**4**) were carried out using a Gemini diffractometer and the related analysis software.[66] An absorption correction based on the crystal faces was applied to the data sets (*analytical*).[67] The structure was solved by direct methods using the SIR97 program[68] combined with Fourier difference syntheses and refined against F using reflections with [$I/\sigma(I)$ > 3] with the CRYSTALS program.[68,69] All atomic displacement parameters for non-hydrogen atoms have been refined with anisotropic terms. The hydrogen atoms were theoretically located on the basis of the conformation of the supporting atom and refined keeping restraints (*riding mode*). Complexes **3** and **4** contain accessible solvent voids, with highly disordered solvent molecules, which have been removed by the SQEEZE program.[70]

Complexes **1** and **2** show a significant disorder in their crystal structure, a disorder higher for **2** than for **1**. For Tb1 in **1**, 12 of 18 fluoride atoms are defined in two positions; the C18, C22, C23, and C27 carbon atoms have six fluoride atoms each instead of three for defining a CF_3 molecule. For Y1 and Y2 in **2**, nine and 12 of 18 fluoride atoms are defined in two positions, respectively. C117, C123, C127 for Y1 and C213, C218, C223, C227 for Y2 have six fluorides each. The disorder on the CF_3 molecules is commonly encountered in the coordination complexes. The heptane molecule close to a symmetry element is disordered over two positions. The NIT2Py connected to Y2 also has a disorder on the four methyl groups, which are defined on two positions. For all these reasons, the R1 and wR2 reliability factor for **2** (R1 = 0.0788 and wR2 = 0.2194) are higher than for **1** (R1 = 0.0523 and wR2 = 0.1437). The hydrogen atoms are placed arbitrarily during the refinement.

Magnetic Measurements. Magnetic susceptibility data (2−300 K) were collected on powdered polycrystalline samples on a Quantum Design MPMS-XL SQUID magnetometer under an applied magnetic field of 0.1 T. Alternating current measurements were performed in the 2−10 K range using a 2.7 G ac field oscillation in the 1−1500 Hz range. Magnetization isotherms were collected at 2 K between 0 and 5 T. All data were corrected for the contribution of the sample holder and the diamagnetism of the samples estimated from Pascal's constants.[71]

Luminescence and Raman Spectroscopy. Luminescence and Raman spectroscopy measurements were carried out using a Renishaw inVia imaging microscope system. Excitation sources were a 488 nm and a 514 nm argon ion laser for luminescence experiments and a 782 nm diode laser for the Raman experiments. The microscope was used to focus the light onto a spot of approximately 1 μm in diameter and to collect the scattered light. The backscattered Raman light was detected with a Peltier-cooled CCD detector. Sample temperatures were controlled with a Linkam microscope cryostat between 80 and 290 K. All spectra were unpolarized and corrected for spectrometer response. The luminescence band maxima E_{max} are determined using the least-squares fit of a Gaussian to the top 10−15% of each band.

The Raman band maxima are determined using the least-squares fit of a Gaussian to the top 20−25% of each band. Maxima are given with a maximum standard deviation of 0.1 cm^{-1}. The relative intensity of 100% is attributed to the most intense band of the spectra.

RESULTS

Crystal Structures. The crystal data and refinement parameters for compounds **1**−**4** are summarized in Table 1. Selected bond lengths and angles are given in Table 2.

[M(hfac)$_3$NIT2Py]·0.5C$_7$H$_{16}$ (M = Tb(III) or Y(III)). [Tb(hfac)$_3$NIT2Py]·0.5C$_7$H$_{16}$ (**1**) crystallizes in the $P2_1/n$ monoclinic space group as was previously reported by Li et al.[51] While **1** is isostructural with the gadolinium derivative [Gd(hfac)$_3$NIT2Py]·0.5C$_7$H$_{16}$ reported by Gatteschi et al.,[62] complex **2** was found to crystallize in the $P\bar{1}$ triclinic space group. The asymmetric unit of **2** consists of two [Y(hfac)$_3$NIT2Py] molecules and one heptane molecule, in general positions, corresponding to two independent entities in contrast to **1**. However, the two [Y(hfac)$_3$NIT2Py] molecules have structural features close to those found for the terbium derivative (**1**). The Y(III) ion is coordinated to six oxygen from the hfac ligands, one oxygen from the NO group, and one nitrogen atom from the pyridine group (Figure S2). The coordination sphere is a deformed square antiprism. The Y−O bond lengths are between 2.258(5) and 2.365(5) Å for Y1 and between 2.270(5) and 2.381(6) Å for Y2, whereas the longer Y−N bond length is 2.609(6) and 2.625(5) Å for Y1 and Y2, respectively. The O−Y−O angles are between 70.4(2)° and 144.4(2)° and between 68.9(2)° and 145.9(2)° for Y1 and Y2, respectively, while the O−Y−N angles are in the range 70.7(2)−146.0(2)° for Y1 and in the range 70.0(2)−146.9(2)° for Y2. The two minima O−Y−N values correspond to the chelating NIT2Py angles to Y1 and Y2. The NIT2Py radical shows normal bond lengths and angles.[72,73] The pyridine and nitronyl nitroxide (ONCNO) moieties make a dihedral angle of 20.2(4)° and 22.6(4)° respectively for Y1 and Y2, which are smaller than the 26.8° reported for **1**.[51]

As the crystal cells contain in both case four [M(hfac)$_3$NIT2Py] molecules and two heptane molecules, the crystal packing of compound **2** is significantly more compact; the cell volumes are 3995.2(14) and 3894.6(6) Å^3 for **1** and **2**, respectively. The crystal packing of **1** and **2** resulted in well-separated [M(hfac)$_3$NIT2Py] with the heptane solvent molecules inserted in between (Figures S3 and S4). The shortest intermolecular Tb···Tb distance was reported as 9.273 Å.[51] In **2** the shortest intermolecular Y2···Y2 and Y1···Y1 distances are 8.673(1) and 9.010(1) Å, respectively, and the shortest intermolecular Y1···Y2 distance is 9.755(1) Å. In both compounds the shortest intermolecular distances between the uncoordinated NO groups are greater than 7 Å.

dx.doi.org/10.1021/ic500779y | Inorg. Chem. XXXX, XXX, XXX−XXX

[M(acac)$_3$NIT2Py]·0.5H$_2$O (M = Tb(III) or Y(III)). The crystal structures of complexes **3** and **4** are isostructural and crystallize in the *C*2/*c* monoclinic space group (Table 1). The asymmetric unit consists of one [M(acac)$_3$NIT2Py] molecule and a half water molecule located on a symmetry plane.

Like for **1** and **2**, the metal center (Tb, Y) ion is coordinated to six oxygen atoms of acac ligands, one oxygen atom from a NO group, and one nitrogen atom from the pryridyl group. The coordination sphere is a deformed square antiprism geometry. In compound **3** (Figure 2) the Tb1−O bond lengths

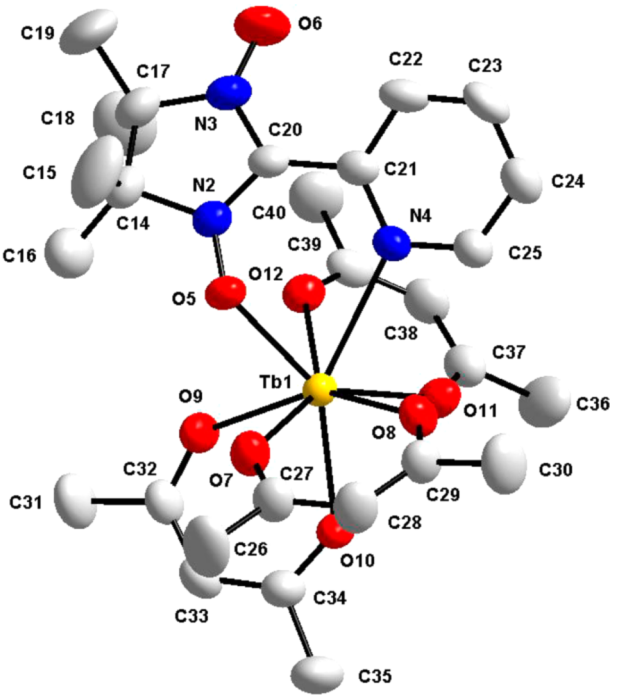

Figure 2. Representation of complex **3**. Ellipsoids are represented at the 50% probability level for all atoms. Hydrogen atoms are omitted for clarity.

are in the range 2.321(3)−2.404(3) Å, whereas the unique Tb1−N4 bond length is 2.702(3) Å. The O−Tb1−O angles are between 70.00(10)° and 147.56(10)°, while the O−Tb1−N4 angles are in the range 66.96(9)−147.88(10)°; the minimum O−Tb1−N4 value corresponds to the chelating NIT2Py angle to Tb(III). In compound **4** the Y1−O bond lengths are in the range 2.302(3)−2.380(3) Å, whereas the unique Y1−N4 bond length is 2.689(3) Å. The O−Y1−O angles are between 70.06(9)° and 148.14(9)°, while the O−Y1−N4 angles are in the range 67.16(9)−147.09(9)°; the minimum O−Tb1−N4 value corresponds to the chelating NIT2Py angle to Y(III). Like for **1** and **2**, NIT2Py shows normal bond length and angles.[72,73] The pyridine and nitronyl nitroxide (ONCNO) moieties make a dihedral angle of 27.2(3)° and 26.4(3)° respectively for **3** and **4**.

The crystal packing of **3** and **4** is identical, as the differences in crystal cell volume are meaningless in comparison with compounds **1** and **2**. The crystal packing may be described as a two-dimensional network developing parallel to the *ab* plane through intermolecular hydrogen bonds connecting the [M(acac)$_3$NIT2Py] entities via the crystallized water molecules, the oxygen of the acac ligand, and the methyl groups of the imidazolyl moiety (Figure S7). The [M(acac)$_3$NIT2Py] are also paired by hydrogen bonds involving an oxygen atom of an acetylacetonate ligand and the pyridine moiety of a second entity (Figures S5 and S6). In **3** the shortest intermolecular Tb···Tb distance is 8.097 Å. In **4** the shortest intermolecular Y···Y is 8.066 Å. The shortest intermolecular distances between an uncoordinated NO group and a Tb ion and between two uncoordinated NO are greater than 6 Å.

Magnetic Properties. *[Tb(hfac)$_3$NIT2Py]·0.5C$_7$H$_{16}$*. The magnetic behavior of **1** was found to be as reported.[51] The χT value at 300 K is in agreement with uncoupled Tb(III) and the radical. Upon cooling, χT decreases first, then from 40 K increases to reach a maximum at 10 K, then decreases on further cooling. The field dependence of the magnetization for **1** does not reach the saturation value due to magnetic anisotropy. The ac measurements under a zero direct-current (dc) field with an alternating current (ac) field of 3 Oe indicated slow relaxation of the magnetization with an energy barrier of Δ/k_B = 17.1 K and preexponential factor $\tau_0 = 9.56 \times 10^{-7}$ s [$\tau = \tau_0 \exp(\Delta/K_BT)$].

[Tb(acac)$_3$NIT2Py]·0.5H$_2$O ***(3)***. At 300 K the χT value is 11.78 emu·K·mol^{-1}, in good agreement with a Tb(III) ion ($^7F_6$ and g = 3/2) and a free radical that is not interacting. Upon cooling, χT slowly and continuously decreases as shown in Figure 3 to finally reach a value of 6.94 emu·K·mol^{-1} at 2 K.

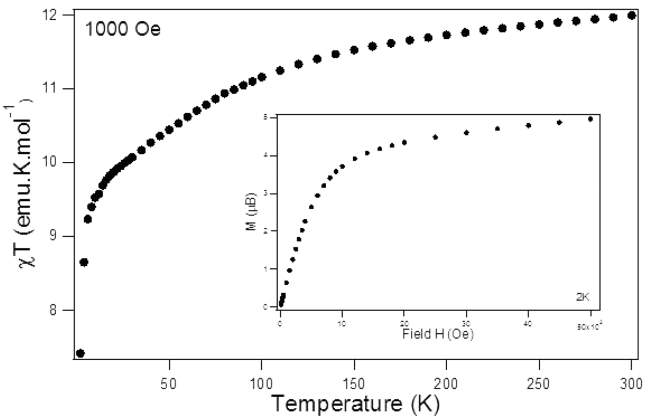

Figure 3. Plot of χT vs T under an applied field of 1000 Oe, with magnetic dependence of the magnetization at 2 K for **3**.

The field dependence for **3** was performed at 2 K in the field range of 0−50 kOe. Upon increasing the magnetic field, the magnetization increases to reach a value of 4.91 μ_B, as shown in Figure 4.

To examine the spin dynamics of complex **3**, ac measurements have been carried out in the range 2−10 K with an ac field of 3 Oe at various frequencies and under dc magnetic fields of 0, 1000, and 3500 Oe. The temperature dependence of the in-phase (χ') and out-of-phase (χ'') ac susceptibilities is frequency dependent below 4 K, regardless of the magnetic field (Figures S9 and S10 and Figure 4). In contrast with compound **1** there are no maxima visible down to 2 K under a zero dc magnetic field. Under a dc magnetic field of 1000 Oe (Figure S9a and b) and 3500 Oe (Figure S10a and b), **3** exhibits maxima values. The frequency dependence of the χ'' peak was fitted by the Arrhenius law $\tau = \tau_0 \exp[\Delta/(k_BT)]$ in which T is the temperature of the maximum χ'' at different frequencies and $\tau = 1/2\pi\nu$. For measurement under a dc magnetic field of 1000 Oe this gives the preexponential factor $\tau_0 = 10^{-7}$ s, and the energy barrier for the relaxation of the magnetization Δ/k_B = 21.18 K with an R factor of 0.9722

dx.doi.org/10.1021/ic500779y | Inorg. Chem. XXXX, XXX, XXX−XXX

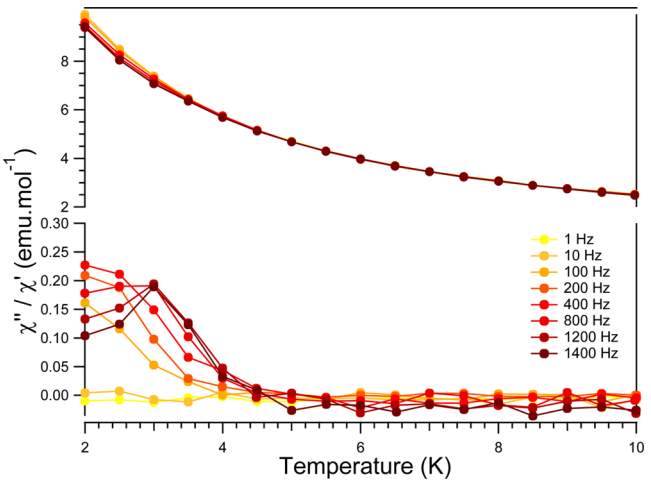

Figure 4. Temperature dependence of the in-phase (top) and out-of-phase (bottom) ac magnetic susceptibility for compound **3** in a 0 Oe dc field with an oscillating field of 3 Oe. The solid lines are a guide for the eye.

(Figure S9c) suggests an SMM behavior. For measurement under a dc magnetic field of 3500 Oe this gives the pre-exponential factor $\tau_0 = 3 \times 10^{-8}$ s, and the energy barrier for the relaxation of the magnetization is $\Delta/k_B = 26.036$ K with an R factor of 0.9980 (Figure S10c).

[Y(acac)$_3$NIT2Py]·0.5H$_2$O (4). At 300 K the χT value for **4** is 0.415 emu·K·mol^{-1}, in good agreement with the expected value for one radical (Figure S11). Upon cooling, χT decreases slowly down to 30 K, then decreases abruptly to reach a value of 0.166 emu·K·mol^{-1} at 2 K. The experimental curve has been well fitted with a Curie–Weiss law for one radical ($s = 1/2$) to give $\theta = -3.1$ K, which confirms the weak radical–radical antiferromagnetic intermolecular interaction.

Raman Spectroscopy. Raman spectra at variable temperature were recorded for [Tb(hfac)$_3$NIT2Py]·0.5C$_7$H$_{16}$ (**1**), [Y(hfac)$_3$NIT2Py]·0.5C$_7$H$_{16}$ (**2**), and the uncoordinated NIT2Py radical between 80 and 300 K for Raman shifts between 100 and 2000 cm^{-1}. Raman shifts given in the following correspond to values obtained at 80 K. No Raman data on the uncoordinated NIT2Py were found in the literature. The data have been compared to the NITBzImH radical (2-(2-benzimidazolyl)-4,4,5,5-tetramethylimidazoline-1-oxyl-3-oxide) characterized by Raman spectroscopy, a radical similar to NIT2Py.[29]

Figure S12a shows the Raman spectra of **1** between 80 and 300 K. Spectra are normalized on the most intense band to simplify the comparison at variable temperature.

The Raman spectra between 80 and 300 K show no significant change aside from higher resolution at lower temperature for some bands. Complex **1** does not show any phase transitions based on the Raman spectra. Some Raman bands shift to slightly lower frequencies as the temperature increases. The Raman bands between 600 and 1600 cm^{-1} correspond essentially to vibrational modes of the NIT2Py radical. This observation can be confirmed by the variable-temperature Raman spectra of the uncoordinated NIT2Py radical. The vibrational frequencies of uncoordinated NIT2Py (616, 991, 1067 cm^{-1}, ...) are lower by a few cm^{-1} than for the coordinated NIT2Py in **1** (621, 1002, 1071 cm^{-1}, ...).

Assignments are limited to comparisons with the literature. A comparison of Raman frequencies for the uncoordinated NIT2Py radical and [Tb(hfac)$_3$NIT2Py]·0.5C$_7$H$_{16}$ can be made (uncoordinated NIT2Py/[Tb(hfac)$_3$NIT2Py]·0.5C$_7$H$_{16}$). The bands at 616/621, 995/1011, 1572/1575, and 1589/1596 cm^{-1} are assigned as modes of the pyridine group.[74,75] Pyridine shows Raman bands at 603/622, 991/1002, 1029, 1067/1071, 1213/1219, 1482, and 1583 cm^{-1}.[29,74] The bands at 1418/1425, 1469/1473, and 1521/1528 cm^{-1} and the band at 1167 cm^{-1} for **1** correspond to the imidazolyle ring stretching frequencies.[76] The Raman bands at 1521/1528 and 1469/1473 cm^{-1} can be attributed to the ν(O–N=C) stretching frequency.[76,77] The ν(N–O$^{\bullet}$) stretching frequency is given as approximately 1370 cm^{-1} in the literature.[78] Two bands are observed in this range, at 1365 and 1376 cm^{-1}, for uncoordinated NIT2Py and at 1370 cm^{-1} for **1**. The δ(C–C–C) bending frequencies of the imidazolyl ring are reported at 204, 271, and 318/319 cm^{-1}.[76] The ν(Tb–O) and ν(Tb–N) stretching frequencies are not easily assigned through comparisons with the literature.[79]

The Raman spectra of **2** have been measured between 80 and 300 K and are very similar to those of **1**. A shift of the Raman maxima to lower frequencies as the temperature increases is observed for **2**, again similar to **1**. The vibrational modes assigned to **1** can also be assigned for **2**.

The values of some vibrational modes previously assigned for **1** can be assigned for **2** as the pyridine vibration modes of the pyridine group at 621, 1008, 1577, and 1596 cm^{-1}. The imidazolyle ring stretching frequencies are observed at 1426, 1473, 1524, and 1168 cm^{-1}, the δ(C–C–C) bending frequency of the imidazolyle ring at 210, 277, and 326 cm^{-1}, and the ρ_r rocking in the plane of the CH$_3$ methyl groups at 871 cm^{-1}.

The Raman spectra of **3** have been measured in the temperature range between 78 and 293 K. A slight shift of the Raman bands to lower energies as the temperature increases is observed, similar to **1** and **2**. Changing the ancillary ligands should lead to some differences between the Raman spectra of **1** and **3**. The Raman bands measured for **3** are relatively broad, but spectra of **3** show similarities with **1** and **2**. The ν(Tb–O) and ν(Tb–N) stretching frequencies are again not easily discernible by comparison with the literature.[79]

The frequencies of some modes previously assigned for **1** can be assigned for the pyridine group in **3** at 624, 1004, and 1589 cm^{-1}. The peak at 1577 cm^{-1} is not discernible. The imidazolyle ring stretching frequencies at 1419, 1454, 1513, and 1173 cm^{-1}, the δ(C–C–C) bending frequency of the imidazolyle ring at 218 and 320 cm^{-1}, and the ρ_r rocking in the plane of the CH$_3$ methyl groups at 873 cm^{-1} are assigned. The band corresponding to the ν(N–O$^{\bullet}$) stretching mode is most likely at 1363 cm^{-1}.

The Raman spectra of **4** have been measured in the temperature range between 80 and 300 K. A slight shift of the Raman bands to lower frequencies as the temperature increases is observed, again similar to **1** and **2**, with corresponding assignments.

Luminescence Spectroscopy. Figure 5a shows the luminescence spectra of [Tb(hfac)$_3$NIT2Py]·0.5C$_7$H$_{16}$ (**1**) between 80 and 300 K. Two energy ranges are characterized: the first between 10 000 and 15 400 cm^{-1}, which corresponds to the luminescence of the NIT2Py radical.[28] In this area, a broad band with three maxima, E_{maxA}, E_{maxB}, and E_{maxC}, at approximately 14 525, 13 070, and 11 700 cm^{-1} is observed at 80 K. The second energy range between 15 400 and 20 000 cm^{-1} corresponds to f–f transitions of Tb(III). The spectra of **1** at room temperature and 270 K show three band maxima at

dx.doi.org/10.1021/ic500779y | Inorg. Chem. XXXX, XXX, XXX–XXX

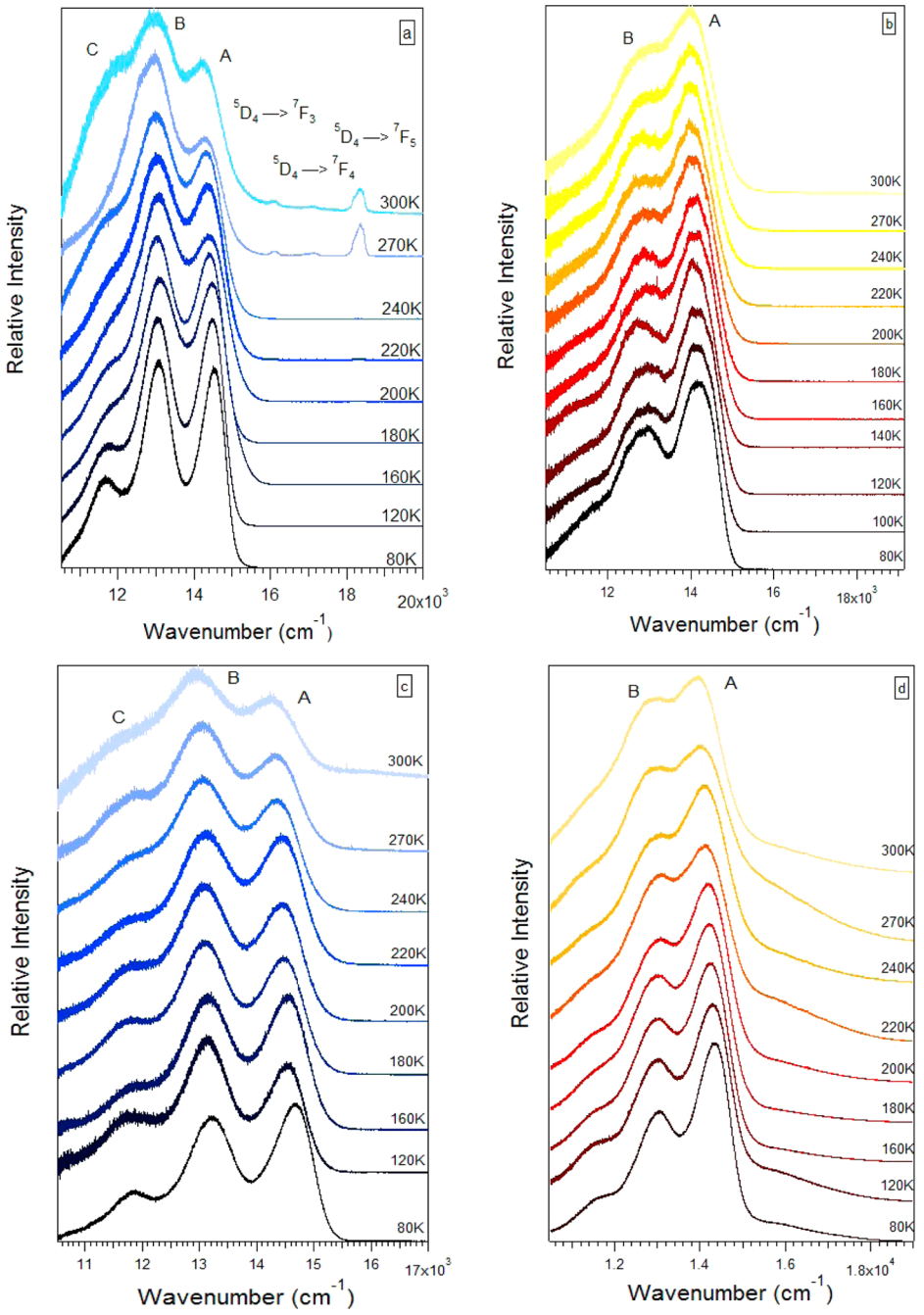

Figure 5. Luminescence spectra at variable temperature (80–300 K) of (a) **1**, (b) **3**, (c) **2**, and (d) **4**. The luminescence spectra are offset along the *y*-axis for clarity. The bands were assigned according to the literature for Tb(III).

approximately 18 360, 17 130, and 16 100 cm^{-1}. These three maxima correspond to luminescence transitions from the $^5D_4$ excited state to the $^7F_5$, $^7F_4$, and $^7F_3$ states of Tb(III).[80] Tb(III) luminescence is not visible at temperatures between 80 and 240 K. At 270 K, the intensity of the f–f transitions is significant and decreases slightly at 300 K.

The resolution of the uncoordinated NIT2Py luminescence spectra is not as good as for the spectra of **1**. The spectra show two luminescence maxima at approximately 14 050 and 12 950 cm^{-1} and a shoulder at lower energy visible at 80 K. Four maxima are reported at 5 K for the uncoordinated NIT2Py radical, at 14 090, 13 570, 11 750, and 11 010 cm^{-1}.[29] Similar band maxima have been reported for uncoordinated NIT radicals in the solid state.[40] The maxima for uncoordinated NIT2Py radical are at somewhat different energy than when coordinated to Tb(III) ions. The maxima for **1** are shifted to 14 525 and 13 070 cm^{-1} at 80 K, differences of approximately 435 and 500 cm^{-1}, respectively. Similar shifts of the luminescence band maxima for uncoordinated and coordinated ligands have already been reported in the literature for Gd(III) complexes with three hfac ligands and one NITBzImH radical.[6] The shift of the luminescence maxima has been attributed to a metal–ligand charge transfer (MLCT) effect.[6] The similarities between Gd(III) and Tb(III) complexes with NIT2Py and NITBzImH radicals illustrate that the luminescence behavior observed for [Tb(hfac)$_3$NIT2Py]·0.5C$_7$H$_{16}$ is similar to that of Gd(hfac)$_3$NITBzImH.[6]

dx.doi.org/10.1021/ic500779y | *Inorg. Chem.* XXXX, XXX, XXX–XXX

Table 3. Variation of the Experimental and Calculated Luminescence Band Maxima E_{maxA}, E_{maxB}, ΔE_{max}, E_{maxA}Th, E_{maxB}Th, and ΔE_{max}Th in Wavenumber Units (cm^{-1}) from the Luminescence Spectra between 80 and 300 K of 1

temperature (K)	E_{maxA} (cm^{-1})	E_{maxB} (cm^{-1})	ΔE_{max} (cm^{-1})	E_{maxA}Th (cm^{-1})	E_{maxB}Th (cm^{-1})	ΔE_{max}Th (cm^{-1})
80	14 525	13070	1455	14520	13075	1445
120	14 475	13050	1425	14474	13054	1420
160	14 465	13005	1360	14446	13078	1368
180	14 400	13030	1370	14385	13025	1360
200	14 385	13065	1320	14343	13067	1284
220	14 360	13050	1310	14350	13038	1312
240	14 300	13000	1300	14305	13000	1305
270	14 270	13020	1250	14250	13030	1220
300	14 200	12960	1240	14196	12940	1256

Table 4. Variation of the Experimental and Calculated Luminescence Band Maxima E_{maxA}, E_{maxB}, ΔE_{max}, E_{maxA}Th, E_{maxB}Th, and ΔE_{max}Th in Wavenumber Units (cm^{-1}) from the Luminescence Spectra between 80 and 300 K of 3

temperature (K)	E_{maxA} (cm^{-1})	E_{maxB} (cm^{-1})	ΔE_{max} (cm^{-1})	E_{maxA}Th (cm^{-1})	E_{maxB}Th (cm^{-1})	ΔE_{max}Th (cm^{-1})
78	14 448	13 116	1332	14 443	13 137	1306
103	14 404	13 095	1309	14 399	13 132	1267
123	14 350	13 055	1295	14 330	13 081	1249
143	14 288	13 058	1230	14 299	13 074	1225
163	14 257	13 078	1179	14 233	13 074	1159
183	14 181	13 050	1131	14 189	13 112	1077
203	14 176	13 141	1035	14 160	13 100	1060
223	14 151	13 161	990	14 131	13 090	1041
243	14 098	13 127	971	14 122	13 085	1037
273	14 041	13 126	915	14 090	13 085	1005
293	13 960	13 137	823	13 981	13 075	906

Table 5. Variation of the Experimental and Calculated Luminescence Band Maxima E_{maxA}, E_{maxB}, ΔE_{max}, E_{maxA}Th, E_{maxB}Th, and ΔE_{max}Th in Wavenumber Units (cm^{-1}) from the Luminescence Spectra between 80 and 300 K of 2

temperature (K)	E_{maxA} (cm^{-1})	E_{maxB} (cm^{-1})	ΔE_{max} (cm^{-1})	E_{maxA}Th (cm^{-1})	E_{maxB}Th (cm^{-1})	ΔE_{max}Th (cm^{-1})
80	14 675	13 220	1455	14 666	13 220	1446
120	14 540	13 140	1400	14 542	13 131	1411
160	14 550	13 155	1395	14 538	13 133	1405
180	14 470	13 095	1375	14 470	13 090	1380
200	14 445	13 090	1355	14 448	13 090	1358
220	14 440	13 115	1330	14 446	13 110	1336
240	14 345	13 060	1285	14 347	13 060	1287
270	14 330	13 050	1280	14 333	13 050	1283
300	14 235	12 960	1275	14 247	12 966	1281

For uncoordinated NIT2Py radical, the energy difference between the two luminescence bands is approximately 1100 cm^{-1}. The corresponding difference is approximately 1455 cm^{-1} at 80 K for the radical coordinated to Tb(III). This energy difference between luminescence maxima E_{maxA} and E_{maxB} (noted ΔE_{max}) for **1** decreases between 80 and 300 K from 1455 cm^{-1} to 1240 cm^{-1}, as shown in Table 3 and Figure S13a. The two luminescence bands shift to lower energies between 80 and 300 K, by approximately 325 cm^{-1} from 14 525 to 14 200 cm^{-1} for E_{maxA} and by 110 cm^{-1} for E_{maxB}, where the maximum oscillates between 13 070 and 12 960 cm^{-1} as the temperature increases. The intensities of E_{maxA} and E_{maxB} are approximately equal between 80 and 160 K, but the intensity ratio changes at higher temperature, where E_{maxB} becomes slightly more intense than E_{maxA}, particularly for the spectrum at 270 K. The maximum E_{maxC} between 11 700 and 11 800 cm^{-1} is observed as a shoulder in the temperature range between 300 and 160 K.

Figure 5b shows the luminescence spectra of [Tb(acac)$_3$NIT2Py]·0.5H_2O (**3**) between 78 and 293 K. In contrast to **1**, only one energy range is characterized, between 10 000 and 15 400 cm^{-1}, corresponding to the luminescence of the NIT2Py radical.[28] In this area, two luminescence band maxima, E_{maxA} and E_{maxB}, at approximately 14 165 and 12 923 cm^{-1} are observed at 78 K. A shoulder can be observed at lower energy, corresponding to the third luminescence band observed in **1**, but the resolution is not good enough to determine E_{maxC}. The energy range between 15 400 and 20 000 cm^{-1} corresponding to the f–f luminescence of the Tb(III) metal center does not show any luminescence band at any temperature, in contrast to **1**.

The two band maxima at 78 K show shifts to higher and lower energies compared to uncoordinated NIT2Py ligand,[29] with an approximate variation +50 cm^{-1} for E_{maxA} from 14 090 to 14 137 cm^{-1} and −590 cm^{-1} for E_{maxB} from 13 570 to 12 980 cm^{-1}. The change from hfac to acac ligands leads to decreases of approximately 388 and 90 cm^{-1} for E_{maxA} and E_{maxB}, respectively, with approximate variations of 3% for E_{maxA} and 0.5% for E_{maxB}. The band maxima E_{maxA} shift to lower energy by approximately 177 cm^{-1} (from 14 137 cm^{-1} to 13 960 cm^{-1}

dx.doi.org/10.1021/ic500779y | Inorg. Chem. XXXX, XXX, XXX–XXX

Table 6. Variation of the Experimental and Calculated Luminescence Band Maxima E_{maxA}, E_{maxB}, ΔE_{max}, E_{maxA}Th, E_{maxB}Th, and ΔE_{max}Th in Wavenumber Units (cm^{-1}) from the Luminescence Spectra between 80 and 300 K of 4

temperature (K)	E_{maxA} (cm^{-1})	E_{maxB} (cm^{-1})	ΔE_{max} (cm^{-1})	E_{maxA}Th (cm^{-1})	E_{maxB}Th (cm^{-1})	ΔE_{max}Th (cm^{-1})
78	14 340	13 043	1297	14 338	13 021	1317
120	14 290	13 013	1277	14 295	13 000	1295
160	14 240	13 020	1220	14 198	12 980	1218
180	14 208	13 024	1184	14 216	13 001	1214
200	14 186	13 078	1108	14 195	13 057	1138
220	14 104	13 095	1004	14 090	13 000	1090
240	14 087	13 098	989	14 101	13 056	1045
270	13 995	13 057	938	13 934	13 033	984
293	13 926	13 014	912	13 899	12 965	935

between 78 and 293 K), corresponding to approximate variations of 1%, as shown in Table 4 and Figure S13b, while E_{maxB} remains constant at approximately 12 980 cm^{-1}. The variation between the two band maxima is higher for **3** than for **1**, 274 cm^{-1} compared to 215 cm^{-1}. The intensity of E_{maxA} is higher by a factor of 2 than E_{maxB} for temperatures between 78 and 293 K. The intensity of the shoulder corresponding to E_{maxC} remains constant over the temperature range studied.

Figure 5c shows the luminescence spectra of [Y(hfac)$_3$NIT2Py]·0.5C_7H_{16} (**2**) between 80 and 300 K. As expected, no luminescence from the Y(III) metal centers is observed in the recorded energy range. The luminescence bands of the radical are between 10 000 and 15 400 cm^{-1}, similar to complex **1**, although the luminescence maxima are slightly higher in energy, as shown in Table 5 and Figure S13c. At 80 K, three luminescence maxima are observed at approximately 14 675, 13 220, and 11 870 cm^{-1} for E_{maxA}, E_{maxB}, and E_{maxC}, respectively. E_{maxC} is not easily discernible at higher temperature. These three maxima are similar in energy to the NIT2Py radical. Shifts of E_{maxA}, E_{maxB}, and E_{maxC} are observed, again similar to **1**. The three band maxima at 80 K show larger shifts to higher energies compared to uncoordinated NIT2Py radical,[29] with an approximate variation of 585 cm^{-1} for E_{maxA} from 14 090 to 14 675 cm^{-1}, 350 cm^{-1} for E_{maxB} from 13 570 to 13 220 cm^{-1} and 120 cm^{-1} for E_{maxC} from 11750 to 11870 cm^{-1}. The changes from Tb(III) to Y(III) ions show increases by approximately 150 cm^{-1}, 150 and 170 cm^{-1}, for E_{maxA}, E_{maxB} and E_{maxC}, respectively. As shown in Table 4, the band maxima E_{maxA} and E_{maxB} shift to lower energies between 80 and 300 K by approximately 440 cm^{-1} from 14 675 to 14 235 cm^{-1} and 260 cm^{-1} from 13 220 to 12 960 cm^{-1}, corresponding to approximate variations of 3% and 2%, respectively. Complex **2** shows a behavior similar to **1**, shifts of 440 and 325 cm^{-1} for E_{maxA} and of 260 and 110 cm^{-1} for E_{maxB}, respectively. The overall shift of E_{maxB} is less than that for E_{maxA}, and the energy difference between the maxima decreases from 1455 cm^{-1} at 80 K to 1275 cm^{-1} at 300 K. A behavior similar to that for [Tb(hfac)$_3$NIT2Py]·0.5C_7H_{16} is observed, but the variation between the two band maxima is lower for **2** than for **1**, 180 cm^{-1} compared to 215 cm^{-1}. The intensities of E_{maxA} and E_{maxB} are approximately equal between 80 and 220 K, but the intensity ratio changes at higher temperature, where E_{maxB} becomes slightly more intense than E_{maxA}. The intensity of E_{maxC} remains constant over the temperature range studied.

Figure 5d shows the luminescence spectra of [Y(acac)$_3$NIT2Py]·0.5H_2O (**4**) between 78 and 293 K. Again no f−f luminescence is observed in the energy range recorded. Two luminescence maxima, E_{maxA} and E_{maxB}, are given in Table 6. At 80 K, E_{maxA} and E_{maxB} are at approximately 14 165 and 12 923 cm^{-1}. A shoulder can be observed at lower energy, corresponding to the third luminescence band observed in **1** and **3**, but the resolution is not good enough to allow a maximum value to be determined. The two maxima at 78 K show a shift to higher and lower energies compared to the uncoordinated NIT2Py ligand,[29] with an approximate variation by 250 cm^{-1} for E_{maxA} from 14 090 cm^{-1} to 14 340 cm^{-1} and 335 cm^{-1} for E_{maxB} from 13 570 cm^{-1} to 13 043 cm^{-1}. The changes from hfac to acac ligand from **3** to **4** show decreases by approximately 388 and 180 cm^{-1} for E_{maxA} and E_{maxB}, respectively, with approximate variations of 3% for E_{maxA} and 1.5% for E_{maxB}. The changes from Tb(III) to Y(III) ions from **2** to **4** show increases by approximately 203 cm^{-1} and 63 cm^{-1}, for E_{maxA} and E_{maxB}, respectively, with approximate variations of 1.5% for E_{maxA} and 0.5% for E_{maxB}. As shown in Table 6 and Figure S13d, the band maxima E_{maxA} undergoes linear shifts to lower energies between 78 and 293 K by approximately 414 cm^{-1} from 14 340 cm^{-1} to 13 926 cm^{-1}, while E_{maxB} remains constant in energy about 13 050 cm^{-1}. Complex **4** does not show a behavior similar to **3**, but the same behavior as **2**, since only shifts for E_{maxA} are observed in **4**. The variation between the two band maxima is higher for **4** than for **3**, 385 cm^{-1} compared to 274 cm^{-1}, and is higher in **4** than in **2**, 385 cm^{-1} compared to 180 cm^{-1}. The intensity of E_{maxA} is higher by a factor of 3 than E_{maxB} between 78 and 220 K and by a factor of 2 between 220 and 293 K. The intensity of the shoulder corresponding to E_{maxC} remains constant over the studied temperature range.

DISCUSSION

Changing the ancillary ligand leads to different crystal packing and change in the space group, which is not surprising, as steric hindrance in acac is much lower than in hfac. As a consequence, **3** and **4** are not isomorphous with **1** or **2**. The half-molecule of heptane that cocrystallizes in **1** or **2** is replaced by a half-molecule of water in **3** and **4**, leading to the formation of intra- and intermolecular hydrogen bonds. Then, while **1** or **2** may be described as discrete and well-isolated molecules, **3** and **4** can be described as 2D networks due to intermolecular hydrogen bonds. This may be an important difference since the crystal packing influences the magnetic properties.

Differences appear also in the metal−ligand bond lengths. In case of **1** and **2**, the M−O_{hfac} bond lengths are 2.323(4)−2.378(4) Å and 2.296(5)−2.381 Å, respectively. The M−O_{NO} bond lengths are 2.313(4) Å for **1** and 2.258(5) and 2.270(5) Å for **2**. The M−N bond lengths are 2.587(4) Å for **1** and 2.609(6) and 2.625(6) Å for **2**. In these complexes, the M−O_{NO} bond lengths are the shortest M−O bond lengths.

dx.doi.org/10.1021/ic500779y | Inorg. Chem. XXXX, XXX, XXX−XXX

For **3** and **4**, the M−O_{acac} bond lengths are 2.323(3) to 2.364(3) Å and 2.299(3) to 2.342(3) Å, respectively. Compared to M−O_{hfac} bond lengths, there is no significant variation. The M−O_{NO} bond lengths are 2.405(3) and 2.380(3) Å for **3** and **4**, respectively. Compared to M−O_{NO} bond lengths in **1** and **2**, there is an increase of 0.092 Å of the Tb−O_{NO} bond lengths, i.e., 3.7% longer, and an increase of 0.122 and 0.110 Å of the Y−O_{NO} bond lengths, i.e., 5% longer. The M−N bond lengths for **3** and **4** are 2.700(3) and 2.689(3) Å, respectively. Compared to the M−N bond lengths in **1** and **2**, there is an increase of 0.113 Å of the Tb−N bond length, i.e., 4% longer, and an increase of 0.080 and 0.064 Å of the Y−N bond length, i.e., 3% longer. For **3** and **4**, the M−O_{NO} bond lengths are the longest M−O bond lengths.

Metal-β-diketonate bond lengths have already been reported to be unaffected by the change from hfac to acac.[50] However, one may say that here the crystal structures for **1** and **2** were determined at low temperature, 150 and 110 K respectively, whereas the crystal structures of **3** and **4** were determined at room temperature. To strengthen our assumption, the crystal structure of **3** has been further determined at 100 K. The Tb−O_{acac} bond lengths are between 2.321(3) and 2.351(3) Å, the Tb−O_{NO} bond length is 2.405(6) Å, and the Tb−N bond length is 2.679(4) Å. That is, these bond lengths differ by less than ∼0.02 Å at 100 K as compared with those found at room temperature. In contrast, even at low temperature, the metal−radical bond length is still longer by ∼0.1 Å in compound **3** as compared to compound **1**. This is ascribed to the electron-withdrawing effect of the hexafluoroacetylacetonate ancillary ligand, which increases, as expected, the Lewis acidity of the metal center, leading to shorter bond lengths in complex **1** than in complex **2**.

The recent discoveries that the metal−radical strategy may contribute to the energy barrier for reversal of magnetization in lanthanide-based SMMs[54−56] give some potential to the design of single-molecule magnets using nitronyl nitroxide radicals. However, in our case, nitronyl nitroxide radicals act only as chelating ligands, leading to discrete molecules. Further work will look at using nitronyl nitroxide as bridging ligands, as they may contribute to increase both the total spin and the strength of magnetic interactions to enhance properties of SMMs. Compounds **2** and **4** of the diamagnetic Y(III) do not show significant magnetic interest but were studied to have an estimation of the intermolecular interaction and to obtain the response of coordinated nitronyl nitroxide radicals in the luminescence studies.

From the magnetic behavior of **4**, it may be seen, and in agreement with the small negative θ value found for the Curie−Weiss fitting, that weak intermolecular antiferromagnetic interactions are operative in **4** and therefore in **3**, as they are isomorphous. For **1** and **3** the χT values at 300 K, respectively 12.16 and 11.78 emu·K·mol^{-1}, are close and in agreement with that expected. Then upon cooling, the temperature dependence of the product of the magnetic susceptibility with temperature (χT) shows that the Tb(III) and the radical NO moiety are ferromagnetically coupled in **1**,[51] whereas they are antiferromagnetically coupled in **3** (Figure 3). A ferromagnetic interaction was also found in the gadolinium analogue of **1** reported by Gatteschi et al.[62] The nature of the magnetic interaction Ln−NIT has first been considered as dependent only on the lanthanide and not from structural features. A systematic investigation supported that antiferromagnetic interactions were expected for lanthanide ions up to the $4f^5$ electronic configurations but ferromagnetic interactions for higher configurations $4f^6$ to $4f^{10}$.[81] This was ascribed to a spin polarization mechanism involving the 5d and 6s orbitals of the lanthanide.[62,81−83] The ferromagnetic behavior of **1** is in agreement with this mechanism. The antiferromagnetic behavior of **3** may thus be due to the intermolecular antiferromagnetic interactions, evidenced in the isomorphous compound **4**, overcoming the Tb(III)−nitroxide ferromagnetic interaction. Moreover, we have seen that the Tb(III)−nitroxide bond lengths increase significantly in **3** as compared to **1**. This may contribute to decrease the strength of the ferromagnetic coupling and increase the effect of the intermolecular antiferromagnetic interactions, or this may even result in antiferromagnetic coupling. Indeed our previous works with lanthanide−nitroxide compounds have shown that the magnetic interaction may be subject to structural feature, as was evidenced from unprecedented cases of Gd(III)−nitroxide antiferromagnetic interactions[31] and further in some Gd(III)−Cu(II) complexes.[84]

The field dependence of the magnetization for **3** like that for **1** does not reach saturation at 50 000 Oe, 6.7 μ_B (**1**)[57] and 4.9 μB for (**3**), far from the theoretical value (8.87 μ_B). This is ascribed to the strong anisotropy of the Tb(III) ion. Accordingly, the ac measurements show an out-of-phase frequency dependence for **3**, in agreement with a single-molecule magnet behavior as found for **1**. However, the energy barrier for **3** is smaller than found for **1**.[51] The χ'' vs T without an external field (Figure 4) of **1** exhibits maxima values above 2 K, with an energy barrier of about 18 K, while **3** shows only frequency-dependence and no maxima values. At higher applied magnetic field **3** exhibits maxima values like for **1**. The energy barrier of **1** is about 27 K and about 36 K at 1000 and 3500 Oe, respectively, while the energy barrier of **3** is about 21 K and about 27 K at 1000 and 3500 Oe, respectively. These differences may have several origins. First this may be the difference in crystal packing, which contributes to weak intermolecular interactions, as well the Tb(III)−nitroxide bond length, which contributes to weaken the strength of the interaction. Another origin may be the differences in the geometry of the square antiprism of lanthanides ions in **1** and **3**. Indeed, studies on bis(phthalocyanine)lanthanide(III) derivatives have shown that the relaxation speed was slower when the geometry of the metal center was close to the ideal D_{4d} antiprismatic geometry; that is, the distortion between the two regular squares was 45°.[85] For **1**, the two faces O1N3O7O8 and O3O4O6O5 are distorted squares whose average torsion angle is approximately 38.5°. For **3**, the two O5N4O7O8 and O9O10O11O12 are distorted squares whose average torsion angle is approximately 35°. **1** has a geometry closer to the ideal D_{4d} geometry than **3**, consistent with a higher energy barrier.

Radical lanthanide complexes have interesting luminescence properties. Several studies concerning visible luminescence of uncoordinated and coordinated nitroxides were reported[32,33,78,86−88] The electronic structure of nitronyl nitroxide radicals has been probed through luminescence spectroscopy, most recently in solution, and discussed in terms of molecular orbitals calculated with DFT theory.[40] In the following, we focus on the vibronic structure and its temperature variation observed for the title compounds. The luminescence spectra at variable temperature for **1**, **2**, **3**, and **4** show an unusual decrease of the energy difference between luminescence maxima as the temperature increases. This effect

dx.doi.org/10.1021/ic500779y | Inorg. Chem. XXXX, XXX, XXX−XXX

Table 7. Parameter Values Used to Calculate the Luminescence Spectra for Uncoordinated NIT2Py Radical and for Complexes 1, 2, 3, and 4 as the Temperature Increases

	T (K)	E_{00} (cm^{-1})	Γ (cm^{-1})	ν_{k1} (cm^{-1})	ν_{k2} (cm^{-1})	ν_{k3} (cm^{-1})	Δk_1	Δk_2	Δk_3
NIT2Py	80	n/a	n/a	1469	615.8	n/a	1.45	1.4	n/a
1	80	14 620	200	1472.1	621.17	250.88	1.57	1.00	0.90
	120	14 580	215	1471.8	621.03	250.64	1.56	1.00	0.80
	160	14 630	245	1471.1	620.63	250.62	1.58	1.10	0.90
	180	14 580	250	1471.1	620.63	250.62	1.60	1.10	0.90
	200	14 620	255	1470.3	620.24	250.53	1.60	1.30	0.80
	220	14 600	260	1469.2	619.67	250.60	1.60	1.20	0.90
	240	14 560	260	1469.2	619.67	250.60	1.60	1.20	0.90
	270	14 600	260	1468.5	619.47	250.53	1.55	1.30	1.00
	300	14 570	300	1467.5	618.00	249.31	1.60	1.20	1.00
2	80	14 740	190	1473.1	620.89	249.22	1.50	1.00	0.75
	120	14 700	255	1472.1	621.66	250.00	1.70	0.90	1.00
	160	14 675	260	1471.0	621.00	249.86	1.60	0.90	0.90
	180	14 630	290	1469.7	621.57	249.67	1.68	0.90	0.90
	200	14 640	300	1469.3	620.60	249.77	1.65	0.90	1.00
	220	14 640	290	1469.2	620.47	250.19	1.58	1.00	0.90
	240	14 590	305	1468.6	620.14	250.11	1.65	1.15	0.75
	270	14 590	325	1467.8	620.35	250.19	1.68	1.00	0.75
	300	14 510	315	1467.3	620.25	250.64	1.65	1.05	0.95
3	78	14 460	200	1361.0	613.20	248.00	1.20	1.00	0.00
	103	14 450	215	1361.0	613.20	248.00	1.15	1.00	0.40
	123	14 400	225	1365.0	613.20	248.00	1.17	1.00	0.50
	143	14 380	240	1365.0	613.20	248.00	1.17	1.00	0.50
	163	14 380	255	1365.0	613.20	248.00	1.17	1.00	0.50
	183	14 350	270	1365.0	613.20	248.00	1.17	1.00	0.80
	203	14 350	280	1365.0	613.20	248.00	1.18	1.05	0.80
	223	14 350	290	1365.0	613.20	248.00	1.18	1.05	0.80
	243	14 340	300	1365.0	613.20	248.00	1.24	1.07	0.80
	273	14 340	320	1365.0	613.20	248.00	1.24	1.07	0.80
	293	14 310	340	1365.0	613.20	248.00	1.24	1.07	1.00
4	78	14 505	225	1446.6	611.64	258.36	1.23	1.00	1.00
	120	14 480	250	1447.0	611.70	258.00	1.28	1.00	1.00
	160	14 430	270	1447.0	611.70	258.00	1.28	1.00	1.00
	180	14 410	280	1447.0	611.70	258.00	1.27	1.05	0.85
	200	14 400	300	1447.0	611.00	258.00	1.25	1.03	0.85
	220	14 380	320	1444.6	613.49	258.00	1.32	1.10	0.90
	240	14 350	325	1447.0	611.70	258.00	1.25	1.05	0.90
	270	14 340	325	1447.0	611.70	258.00	1.37	1.15	1.10
	293	14 280	340	1444.6	613.49	258.36	1.37	1.15	1.00

is significant, as the energy difference decreases from approximately 1500 cm^{-1} to approximately 1000 cm^{-1}, a surprising change of 500 cm^{-1}. We analyze this unusual effect through calculated luminescence spectra based on harmonic potential energy surfaces, a well-established approach using the time-dependent theory of spectroscopy.[58]

All parameter values used for these calculations are summarized in Table 7. Vibrational frequencies used to calculate the spectra are determined from Raman spectra and do not show the variation by 500 cm^{-1} observed for energy differences in luminescence spectra measured at low and high temperatures, as illustrated in detail in Figure 7. The calculated luminescence spectra are in very good agreement with the experimental spectra especially at temperatures below 240 K, as shown in Figure 6.

The comparison between experimental and calculated ΔE_{max} values in the temperature range from 80 to 300 K is presented for **1** and **3** in Figure 7a and for **2** and **4** in Figure 7b. The ΔE variation shows that luminescence experimental spectra are accurately reproduced for all complexes especially at temperatures lower than 240 K. It is easier to reproduce luminescence spectra for **1** and **2** than for **3** and **4**. At higher temperatures, it is difficult to reproduce experimental luminescence spectra due to the poor resolution. The calculated E_{00} electronic origin parameter shows a decrease for **2**, **3**, and **4** and stays constant for **1** in the temperature range studied. The E_{00} value at 80 K is approximately 14 600, 14 700, 14 500, and 14 500 cm^{-1}, higher by 200, 300, 100, and 100 cm^{-1} for complexes **1**, **2**, **3**, and **4**, respectively, than 14 400 cm^{-1} for the uncoordinated radical.

Offsets along the normal coordinates are similar for all complexes with no significant variations as the temperature changes. Slight variations of less than 10% confirm that there are no strong structural modifications in the complexes, as supported by the information obtained from Raman spectra.

Several parameters are adjusted to reproduce the experimental spectra, namely, the offsets Δ along each normal coordinate and the width Γ of each vibronic line, a value identified as a damping factor in the context of time-dependent

dx.doi.org/10.1021/ic500779y | Inorg. Chem. XXXX, XXX, XXX−XXX

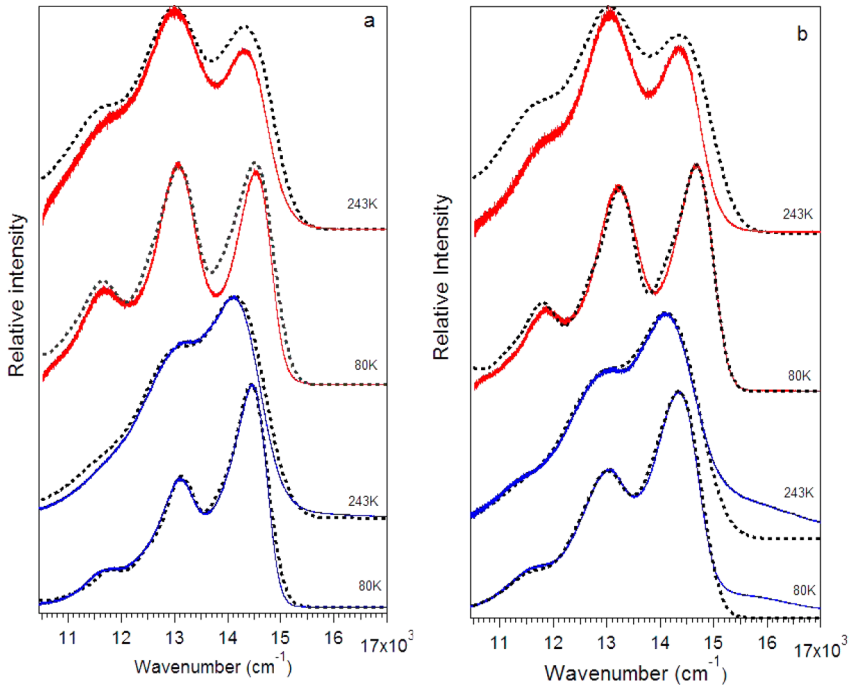

Figure 6. Experimental (solid line) and calculated (dotted line) luminescence spectra at variable temperature (80−300 K) of (a) **1** (top) and **3** (bottom) and (b) **2** (top) and **4** (bottom).

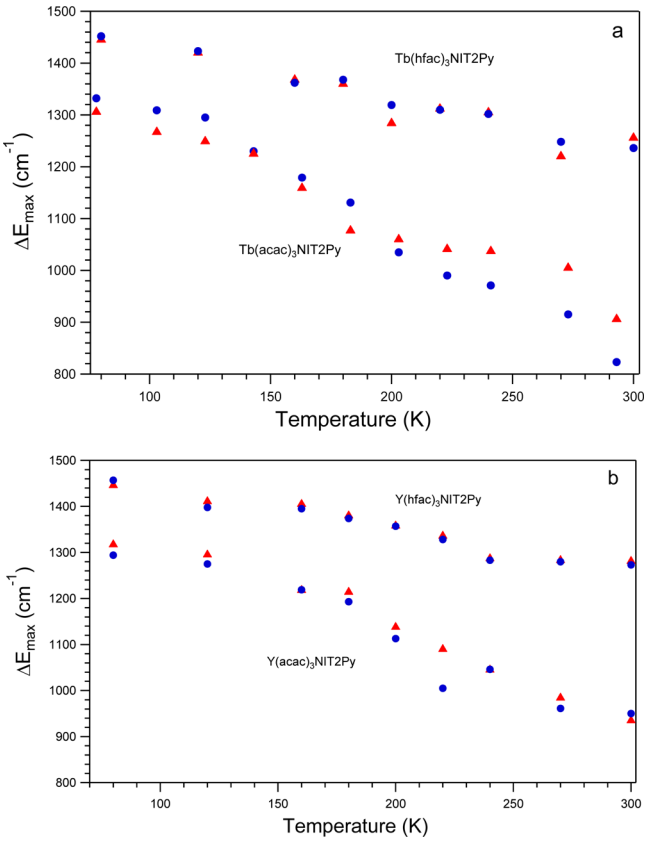

Figure 7. Variations of the ΔE parameter for the experimental (●) and calculated (▲) luminescence spectra as the temperature increases for **1** and **3** (a) and **2** and **4** (b).

theory, a parameter determining the resolution of the calculated spectra.

The energy differences ΔE_{max} in Figure 7 do not correspond to experimental Raman frequencies, a situation reminiscent of the missing mode effect (MIME) discussed in luminescence spectra of many transition metal compounds.[89−91] The MIME frequency observed in the luminescence spectra of these compounds is due to emitting-state distortions along several normal coordinates with different frequencies and is easily rationalized in the time-dependent theory by exploring the products of autocorrelation functions along a single normal coordinate. A formula has been published to calculate the MIME frequency from parameters used to calculate a spectrum, such as the values in Table 7 for the title compounds.[92] Using these values, an increase of the calculated MIME frequency is obtained with increasing temperature, shown in Figure S15, in contrast to the decrease illustrated in Figure 7. The effect observed here is therefore different from the well-established MIME. It involves the magnitude of the widths of vibronic lines in the calculated spectra (parameter Γ), which become less resolved as the temperature increases, ultimately leading to an unresolved envelope with a single maximum, determined by the short-time dynamics. This is illustrated in Figure S16 for spectra calculated only with the highest frequency, 1472 cm^{-1}, mode. For short progressions involving high-frequency modes, a situation typical for ligand-centered transitions, this regime leads to vibronic maxima that move closer together as Γ increases, as shown in Figure S17. The autocorrelation functions in Figure S18 show that the vibrational recurrence disappears for the range of Γ values where the maxima shift most visibly, corresponding to the situation reported here for the title compounds. This effect is illustrated and analyzed for the first time for a series of experimental spectra, documenting the rich variety of physical properties of lanthanide−radical complexes.

dx.doi.org/10.1021/ic500779y | Inorg. Chem. XXXX, XXX, XXX−XXX

CONCLUSION

We have prepared four complexes of terbium(III) or yttrium(III) with a nitronyl nitroxide organic radical and hexafluoroacetylacetonate or acetylacetonate ligands, and we have compared the properties and structures obtained with the two ancillary ligands. Their structural and magnetic properties as well as their luminescence and Raman spectra are compared. The terbium(III) complexes both exhibit single-molecule magnet behavior. For all four complexes the vibronic structure of the luminescence bands cannot be assigned by single vibrational frequencies, and a variation of the vibronic interval occurs with temperature. This effect has to be described with the quantitative variation of all parameters. To the best of our knowledge, it is the first time that such a behavior is reported for lanthanide−radical complexes.

ASSOCIATED CONTENT

Supporting Information

Additional X-ray crystal structures and magnetic ac and dc susceptibilities; Raman and calculated luminescence spectra; Raman shift and peak intensities; crystallographic data in CIF format. This material is available free of charge via the Internet at http://pubs.acs.org.

AUTHOR INFORMATION

Corresponding Authors

*E-mail: christian.reber@umontreal.ca. Fax: +1 514 343 7586. Tel: +1 514 343 7332.

*E-mail: luneau@univ-lyon1.fr. Fax: +33 4 72 43 11 60. Tel: +33 4 72 43 14 18.

Notes

The authors declare no competing financial interest.

ACKNOWLEDGMENTS

The authors thank Francine Bélanger Gariépy for her support in crystal structure determination. A.L. held a CMIRA Explora'doc 2012 fellowship from la Région Rhône-Alpes. The collaborative research was made possible by a grant from the Conseil Franco-Québécois de Coopération Universitaire (CCFQ, administrated by FQRNT, Province of Québec), from la Région Rhône-Alpes through the CMIRA COOPERA 2013 program, and by grants from the Natural Sciences and Engineering Research Council (Canada).

REFERENCES

(1) Sessoli, R.; Tsai, H.-L.; Schake, A. R.; Wang, S.; Vincent, J. B.; Folting, K.; Gatteschi, D.; Christou, G.; Hendrickson, D. N. *J. Am. Chem. Soc.* **1993**, *115*, 1804.

(2) Aromi, G.; Brechin, E. K. *Struct. Bonding* **2006**, *122*, 1.

(3) Christou, G. *Polyhedron* **2005**, *24*, 2065.

(4) Ishikawa, N.; Sugita, M.; Ishikawa, T.; Koshihara, S.; Kaizu, Y. *J. Am. Chem. Soc.* **2003**, *125*, 8694.

(5) Ishikawa, N.; Satoshi, O.; Kaizu, Y. *Angew. Chem., Int. Ed.* **2005**, *44*, 731.

(6) Aronica, C.; Pilet, G.; Chastanet, G.; Wernsdorfer, W.; Jacquot, J. F.; Luneau, D. *Angew. Chem., Int. Ed.* **2006**, *45*, 4659.

(7) Tang, J. K.; Hewitt, I.; Madhu, N. T.; Chastanet, G.; Wernsdorfer, W.; Anson, C. E.; Benelli, C.; Sessoli, R.; Powell, A. K. *Angew. Chem., Int. Ed.* **2006**, *45*, 1729.

(8) Borta, A.; Jeanneau, E.; Chumakov, Y.; Luneau, D.; Ungur, L.; Chibotaru, L. F.; Wernsdorfer, W. *New J. Chem.* **2011**, *35*, 1270.

(9) Iasco, O.; Novitchi, G.; Jeanneau, E.; Wernsdorfer, W.; Luneau, D. *Inorg. Chem.* **2011**, *50*, 7373.

(10) Sessoli, R.; Powell, A. K. *Coord. Chem. Rev.* **2009**, *253*, 2328.

(11) Hewitt, I. J.; Tang, J.; Madhu, N. T.; Anson, C. E.; Lan, Y.; Luzon, J.; Etienne, M.; Sessoli, R.; Powell, A. K. *Angew. Chem., Int. Ed.* **2010**, *49*, 6352.

(12) Blagg, R. J.; Muryn, C. A.; McInnes, E. J. L.; Tuna, F.; Winpenny, R. E. P. *Angew. Chem., Int. Ed.* **2011**, *50*, 6530.

(13) Takamatsu, S.; Ishikawa, T.; Koshihara, S. Y.; Ishikawa, N. *Inorg. Chem.* **2007**, *46*, 7250.

(14) Coutinho, J. T.; Antunes, M. A.; Pereira, L. C. J.; Bolvin, H.; Marcalo, J.; Mazzanti, M.; Almeida, M. *Dalton Trans.* **2012**, *41*, 13568.

(15) Mazzanti, M. *Nat. Chem.* **2011**, *3*, 426.

(16) Antunes, M. A.; Pereira, L. C. J.; Santos, I. C.; Mazzanti, M.; Marcalo, J.; Almeida, M. *Inorg. Chem.* **2011**, *50*, 9915.

(17) Mills, D. P.; Moro, F.; McMaster, J.; van Slageren, J.; Lewis, W.; Blake, A. J.; Liddle, S. T. *Nat. Chem.* **2011**, *3*, 454.

(18) Rinehart, J. D.; Long, J. R. *Dalton Trans.* **2012**, *41*, 13572.

(19) Rinehart, J. D.; Long, J. R. *J. Am. Chem. Soc.* **2009**, *131*, 12558.

(20) Rinehart, J. D.; Harris, T. D.; Kozimor, S. A.; Bartlett, B. M.; Long, J. R. *Inorg. Chem.* **2009**, *48*, 3382.

(21) Feng, X. W.; Liu, J. J.; Harris, T. D.; Hill, S.; Long, J. R. *J. Am. Chem. Soc.* **2012**, *134*, 7521.

(22) Petit, S.; Neugebauer, P.; Pilet, G.; Chastanet, G.; Barra, A. L.; Antunes, A. B.; Wernsdorfer, W.; Luneau, D. *Inorg. Chem.* **2012**, *51*, 6645.

(23) Ruamps, R.; Batchelor, L. J.; Maurice, R.; Gogoi, N.; Jimenez-Lozano, P.; Guihery, N.; de Graaf, C.; Barra, A. L.; Sutter, J. P.; Mallah, T. *Chem.—Eur. J.* **2013**, *19*, 950.

(24) Tancini, E.; Rodriguez-Douton, M. J.; Sorace, L.; Barra, A. L.; Sessoli, R.; Cornia, A. *Chem.—Eur. J.* **2010**, *16*, 10482.

(25) Borta, A.; Gillon, B.; Gukasov, A.; Cousson, A.; Luneau, D.; Jeanneau, E.; Ciumacov, I.; Sakiyama, H.; Tone, K.; Mikuriya, M. *Phys. Rev. B* **2011**, *83*.

(26) Damjanovic, M.; Katoh, K.; Yamashita, M.; Enders, M. *J. Am. Chem. Soc.* **2013**, *135*, 14349.

(27) Baumgartel, N.; Flambard, A.; Kohler, F. H.; Lescouezec, R. *Inorg. Chem.* **2013**, *52*, 12634.

(28) Beaulac, R.; Bussière, G.; Reber, C.; Lescop, C.; Luneau, D. *New J. Chem.* **2003**, *27*, 1200.

(29) Bussière, G.; Beaulac, R.; Bélisle, H.; Lescop, C.; Luneau, D.; Rey, P.; Reber, C. *Top. Curr. Chem.* **2004**, *241*, 97.

(30) Lescop, C.; Belorizky, E.; Luneau, D.; Rey, P. *Inorg. Chem.* **2002**, *41*, 3375.

(31) Lescop, C.; Luneau, D.; Belorizky, E.; Fries, P.; Guillot, M.; Rey, P. *Inorg. Chem.* **1999**, *38*, 5472.

(32) Lescop, C.; Luneau, D.; Bussière, G.; Triest, M.; Reber, C. *Inorg. Chem.* **2000**, *39*, 3740.

(33) Lescop, C.; Luneau, D.; Rey, P.; Bussière, G.; Reber, C. *Inorg. Chem.* **2002**, *41*, 5566.

(34) Petit, S.; Baril-Robert, F.; Pilet, G.; Reber, C.; Luneau, D. *Dalton Trans.* **2009**, 6809.

(35) Cosquer, G.; Pointillart, F.; Jung, J.; Le Guennic, B.; Golhen, S.; Cador, O.; Guyot, Y.; Brenier, A.; Maury, O.; Ouahab, L. *Eur. J. Inorg. Chem.* **2014**, *2014*, 69.

(36) Pointillart, F.; Le Guennic, B.; Cauchy, T.; Golhen, S.; Cador, O.; Maury, O.; Ouahab, L. *Inorg. Chem.* **2013**, *52*, 5978.

(37) Pointillart, F.; Le Guennic, B.; Golhen, S.; Cador, O.; Maury, O.; Ouahab, L. *Chem. Commun.* **2013**, *49*, 615.

(38) Boulon, M. E.; Cucinotta, G.; Luzon, J.; Degl'Innocenti, C.; Perfetti, M.; Bernot, K.; Calvez, G.; Caneschi, A.; Sessoli, R. *Angew. Chem., Int. Ed.* **2013**, *52*, 350.

(39) Cucinotta, G.; Perfetti, M.; Luzon, J.; Etienne, M.; Car, P. E.; Caneschi, A.; Calvez, G.; Bernot, K.; Sessoli, R. *Angew. Chem., Int. Ed.* **2012**, *51*, 1606.

(40) Tretyakov, E. V.; Plyusnin, V. F.; Suvorova, A. O.; Larionov, S. V.; Popov, S. A.; Antonova, O. V.; Zueva, E. M.; Stass, D. V.; Bogomyakov, A. S.; Romanenko, G. V.; Ovcharenko, V. I. *J. Lumin.* **2014**, *148*, 33.

(41) Pointillart, F.; Bernot, K.; Poneti, G.; Sessoli, R. *Inorg. Chem.* **2012**, *51*, 12218.

(42) Caneschi, A.; Gatteschi, D.; Rey, P. *Acc. Chem. Res.* **1989**, *22*, 392.
(43) Caneschi, A.; Gatteschi, D.; Rey, P. *Prog. Inorg. Chem.* **1991**, *39*, 331.
(44) Sutter, J.-P.; Kahn, M. L.; Golhen, S.; Ouahab, L.; Kahn, O. *Chem.—Eur. J.* **1998**, *4*, 571.
(45) Sutter, J.-P.; Kahn, M. L.; Kahn, O. *Adv. Mater. (Weinheim, Ger.)* **1999**, *11*, 863.
(46) Luneau, D.; Rey, P. *Coord. Chem. Rev.* **2005**, *249*, 2591.
(47) Vostrikova, K. E.; Luneau, D.; Wernsdorfer, W.; Rey, P.; Verdaguer, M. *J. Am. Chem. Soc.* **2000**, *122*, 718.
(48) Caneschi, A.; Gatteschi, D.; Lalioti, N.; Sangregorio, C.; Sessoli, R.; Venturi, G.; Vindigni, A.; Rettori, A.; Pini, M. G.; Novak, M. A. *Europhys. Lett.* **2002**, *58*, 771.
(49) Bernot, K.; Pointillart, F.; Rosa, P.; Etienne, M.; Sessoli, R.; Gatteschi, D. *Chem. Commun.* **2010**, *46*, 6458.
(50) Mei, X.-L.; Ma, Y.; Li, L.-C.; Liao, D.-Z. *Dalton Trans.* **2012**, *41*, 505.
(51) Wang, X.-L.; Li, L.-C.; Liao, D.-Z. *Inorg. Chem.* **2010**, *49*, 4735.
(52) Liu, R. N.; Li, L. C.; Wang, X. L.; Yang, P. P.; Wang, C.; Liao, D. Z.; Sutter, J. P. *Chem. Commun.* **2010**, *46*, 2566.
(53) Tian, H. X.; Liu, R. N.; Wang, X. L.; Yang, P. P.; Li, Z. X.; Li, L. C.; Liao, D. Z. *Eur. J. Inorg. Chem.* **2009**, 4498.
(54) Rinehart, J. D.; Fang, M.; Evans, W. J.; Long, J. R. *J. Am. Chem. Soc.* **2011**, *133*, 14236.
(55) Rinehart, J. D.; Fang, M.; Evans, W. J.; Long, J. R. *Nat. Chem.* **2011**, *3*, 538.
(56) Demir, S.; Zadrozny, J. M.; Nippe, M.; Long, J. R. *J. Am. Chem. Soc.* **2012**, *134*, 18546.
(57) Wang, X.; Bao, X.; Xu, P.; Li, L. *Eur. J. Inorg. Chem.* **2011**, *2011*, 3586.
(58) Reber, C.; Zink, J. I. *J. Chem. Phys.* **1992**, *96*, 2681.
(59) Hirel, C.; Vostrikova, K. E.; Pécaut, J.; Ovcharenko, V. I.; Rey, P. *Chem.—Eur. J.* **2001**, *7*, 2007.
(60) Osiecki, J. H.; Ullman, E. F. *J. Am. Chem. Soc.* **1968**, *90*, 1078.
(61) Richardson, M. F.; Wagner, W. F.; Sand, D. E. *J. Inorg. Nucl. Chem.* **1968**, *30*, 1275.
(62) Benelli, C.; Caneschi, A.; Gatteschi, D.; Pardi, L. *Inorg. Chem.* **1992**, *31*, 741.
(63) *APEX2*, Bruker Molecular Analysis Research Tool; Bruker AXS Inc.: Madison, WI, USA, 2006.
(64) Sheldrick, G. M. *SADABS*, Bruker Area Detector Absorption Corrections; Bruker AXS Inc.: Madison, WI, USA, 1996 and 2004.
(65) Sheldrick, G. *Acta Crystallogr. A* **2008**, *64*, 112.
(66) *CrysAlisPro*, O. D. L., Version 1.171.33.46; CrysAlis171.NET, 2009.
(67) De Meulenaar, J.; Tompa, H. *Acta Crystallogr. A* **1965**, *19*, 1014.
(68) Cascarano, G.; Altomare, A.; Giacovazzo, C.; Guagliardi, A.; Moliterni, A. G. G.; Siliqi, D.; Burla, M. C.; Polidori, G.; Camalli, M. *Acta Crystallogr. A* **1996**, *52*, C.
(69) Watkin, D. J.; Prout, C. K.; Carruthers, J. R.; Betteridge, P. W. *CRYSTALS* Issue 11; Chemical Crystallography Laboratory: Oxford, U.K., 1999.
(70) Farrugia, L. *J. Appl. Crystallogr.* **1999**, *32*, 837.
(71) Pascal, P. *Ann. Chim. Phys.* **1910**, *19*, 5.
(72) Depanthou, F. L.; Luneau, D.; Laugier, J.; Rey, P. *J. Am. Chem. Soc.* **1993**, *115*, 9095.
(73) Luneau, D.; Risoan, G.; Rey, P.; Grand, A.; Caneschi, A.; Gatteschi, D.; Laugier, J. *Inorg. Chem.* **1993**, *32*, 5616.
(74) Fang, C.; Wu, G. *Spectrochim. Acta, Part A* **2010**, *77*, 948.
(75) Xiao, C.; Feng, K.; Mo, Y.; Meng, Q.; Zhang, M.; Wan, M.; Zhao, J. *Chem. Phys.* **1998**, *237*, 73.
(76) Mo, Y.-J.; Li, Y.-C.; Zhao, J.-G.; Fen, K.-A.; Xiao, C.-Y.; Wan, M.-X. *J. Magn. Magn. Mater.* **2000**, *213*, 278.
(77) Tsukahara, Y.; Iino, A.; Yoshida, T.; Suzuki, T.; Kaizaki, S. *J. Chem. Soc., Dalton Trans.* **2002**, 181.
(78) Rintoul, L.; Micallef, A. S.; Bottle, S. E. *Spectrochim. Acta, Part A* **2008**, *70*, 713.
(79) Guofa, L.; Tongshun, S.; Yongnian, Z. *J. Mol. Struct.* **1997**, *412*, 75.
(80) Yamashita, K.; Takeuchi, N.; Taniguchi, H.; Yuyama, S.; Oe, K.; Mibuka, N.; Suzuki, A.; Mataki, H. *J. Lumin.* **2009**, *129*, 526.
(81) Kahn, M. L.; Sutter, J. P.; Golhen, S.; Guionneau, P.; Ouahab, L.; Kahn, O.; Chasseau, D. *J. Am. Chem. Soc.* **2000**, *122*, 9566.
(82) Zhang, C. H.; Sun, N. N.; Zhao, X. Y.; Zang, Y. Y.; Guo, Y. L. *Inorg. Chem. Commun.* **2011**, *14*, 166.
(83) Xu, J. X.; Ma, Y.; Liao, D. Z.; Xu, G. F.; Tang, J.; Wang, C.; Zhou, N.; Yan, S. P.; Cheng, P.; Li, L. C. *Inorg. Chem.* **2009**, *48*, 8890.
(84) Costes, J. P.; Dahan, F.; Dupuis, A.; Laurent, J. P. *Inorg. Chem.* **2000**, *39*, 169.
(85) Wang, H.; Wang, K.; Tao, J.; Jiang, J. *Chem. Commun.* **2012**, *48*, 2973.
(86) Godlewska, P.; Gerasymchuk, Y.; Tomachynskii, L.; Legendziewicz, J.; Hanuza, J. *Struct. Chem.* **2010**, *21*, 461.
(87) Tsukahara, Y.; Nakata, H.; Kaizaki, S. *Inorg. Chem.* **2004**, *43*, 4383.
(88) Beaulac, R.; Luneau, D.; Reber, C. *Chem. Phys. Lett.* **2005**, *405*, 153.
(89) Tutt, L.; Tannor, D.; Heller, E. J.; Zink, J. I. *Inorg. Chem.* **1982**, *21*, 3858.
(90) Tutt, L.; Zink, J. I. *J. Am. Chem. Soc.* **1986**, *108*, 5830.
(91) Zink, J. I. *Coord. Chem. Rev.* **2001**, *211*, 69.
(92) Tutt, L. W.; Zink, J. I.; Heller, E. J. *Inorg. Chem.* **1987**, *26*, 2158.